JOURNAL OF AIRCRAFT
Vol. 46, No. 4, July–August 2009

Automatic Transition Prediction in Hybrid Flow Solver, Part 2: Practical Application

Andreas Krumbein*
DLR, German Aerospace Center, D-37073 Göttingen, Germany
Normann Krimmelbein†
Braunschweig University of Technology, D-38106 Brunswick, Germany
and
Geza Schrauf‡
Airbus, D-28199 Bremen, Germany

DOI: 10.2514/1.39738

This article is the second of two companion papers which document the concept and the application of a coupled computational fluid dynamics system which was designed to incorporate the prediction of laminar–turbulent transition into a hybrid Reynolds-averaged Navier–Stokes solver. Whereas the first part deals with the description of the transition prediction methodology and the sensitivities of the coupled system, the second part documents its practical application. The complete coupled system consists of the Reynolds-averaged Navier–Stokes code, a laminar boundary-layer code, and a fully automated local, linear stability code. The system predicts and applies transition locations due to Tollmien–Schlichting and crossflow instabilities using the e^N method based on the two-N-factor approach. The coupled system was designed to be applied to three-dimensional aircraft configurations which are of industrial relevance. The application of the coupled system to a wing–body configuration with a three-element wing consisting of slat, main wing, and flap is described and documented in this paper. The prediction of the laminar–turbulent transition lines was done in a fully automatic manner. It is shown that complex aircraft configurations can be handled without a priori knowledge of the transition characteristics of the specific flow problem.

Nomenclature

b	=	semispan
c	=	local chord length
c_p	=	pressure coefficient
k_{cyc}	=	number of Reynolds-averaged Navier–Stokes cycles for the transition location iteration which represents the interval between two calls of the transition prediction module
M	=	Mach number
n_T	=	global number of transition points
Re	=	Reynolds number
Tu	=	turbulence intensity
x	=	longitudinal coordinate of the configuration in the global coordinate system of the Reynolds-averaged Navier–Stokes solver
x^T	=	longitudinal coordinate value of the transition point
y	=	spanwise coordinate being perpendicular to the longitudinal axis
α	=	angle of attack
δ_F	=	flap deflection angle
δ_S	=	slat deflection angle
η	=	nondimensional spanwise coordinate

Subscripts

CF	=	crossflow
crit	=	critical
j	=	counter of the transition points
TS	=	Tollmien–Schlichting
∞	=	freestream value

I. Introduction

THIS article is the second of two companion papers which document the concept and the application of a coupled computational fluid dynamics (CFD) system which was designed to incorporate the prediction of laminar–turbulent transition into a hybrid Reynolds-averaged Navier–Stokes (RANS) solver. The complete coupled system consists of the RANS code, a laminar boundary-layer code, and a fully automated local, linear stability code. The system predicts and applies transition locations due to Tollmien–Schlichting and crossflow instabilities using the e^N method based on the two-N-factor approach. The coupled system was designed to be applied to three-dimensional aircraft configurations which are of industrial relevance.

Whereas the first part of the combined paper deals with the description of the transition prediction methodology and the sensitivities of the coupled system, the second part documents its practical application. The coupled system is based on the unstructured/hybrid RANS solver TAU [1–4] of the DLR, German Aerospace Center and was designed to be applied to three-dimensional aircraft configurations that are of industrial relevance, and the transition prediction methodology provides two different approaches which are available to be used in different flow situations, for example, attached or separated flow. In the first part of the paper, both approaches are described and tested in detail. The differences in the design of the two

Presented as Paper 413 at the 46th AIAA Aerospace Sciences Meeting and Exhibit, Reno, Nevada, 7–10 January 2008; received 13 July 2008; revision received 26 September 2008; accepted for publication 2 November 2008.

*Research Engineer, Institute of Aerodynamics and Flow Technology, C²A²S²E Center for Computer Applications in AeroSpace Science and Engineering, Bunsenstraße 10; andreas.krumbein@dlr.de. Member AIAA.

†Research Engineer, Institute of Fluid Mechanics, Aerodynamics of Aircraft, Bienroder Weg 3; currently German Aerospace Center, D-38108 Brunswick, Germany, Institute of Aerodynamics and Flow Technology, C²A²S²E Center for Computer Applications in AeroSpace Science and Engineering, Lilienthalplatz 7; normann.krimmelbein@dlr.de.

‡Research and Technology Manager and Senior Research Scientist, Germany Aerodynamics Domain, Airbus Allee 1; geza.schrauf@airbus.com. Senior Member AIAA.

approaches are pointed out and the application of both approaches to different geometries of different complexity is demonstrated. The complete coupled system was applied to a two-dimensional two-element airfoil configuration and a three-dimensional generic full aircraft configuration and the application is described and documented. The focus of the first part of the paper is on the sensitivities of the coupled system and the interactions between the different parts of the system. The differences of the behavior of the two different approaches, the differences in the results they produce, and, most important, the differences of their interaction with the RANS solver, which are significant, are pointed out in the first part.

The second part of the paper deals with the practical application of the complete coupled system to an industrially relevant aircraft configuration in a production environment. The system, with its integrated automatic transition prediction procedure, is applied to a three-dimensional high-lift wing–body aircraft configuration with a three-element wing consisting of slat, main wing, and flap. Only one of the two prediction approaches is used. It is the approach that was designed for current production purposes in industry and which is recommended for wing design work on transport aircraft.

The main objective of the paper is to show that the coupling structure between the hybrid RANS solver and the transition prediction module can be applied to three-dimensional high-lift flows over wings of transport-type aircraft in an automatic manner and in the same way as it was done before, using a different tool chain consisting of a block-structured RANS code, a different laminar boundary-layer code and e^N-database methods [5–7], and that the TAU code provides all technical features that are necessary for the transition prediction on industrially relevant aircraft configurations. It is shown that the prediction approach is ready to be used in an industrial production environment. The article contains results of physical validation work as well as a comparison with results using the tool chain based on block-structured RANS code, which demonstrates the reliability of the underlying transition prediction methodology.

The work presented in this paper covers only transition phenomena that are captured by linear stability theory, that is, Tollmien–Schlichting and crossflow transition.

II. Transition Prediction Coupling Structure

The transition prediction module coupled to the TAU code consists of an infrastructure part inside the RANS solver and a number of external codes which are used for transition prediction purposes. The infrastructure part processes data on the surfaces of the configuration, for example, the extraction of the surface c_p distribution which is then used as input for the laminar boundary-layer code that provides all laminar boundary-layer parameters. Thus, as outlined in detail in the first part of this paper, the grid dependency of the laminar boundary-layer parameters that occurs if one computes them directly inside the RANS computational grid is avoided. The external tools are a streamline-oriented, laminar boundary-layer method for swept, tapered wings [8] and different transition prediction methods. The laminar boundary-layer method solves the compressible, laminar boundary-layer equations for conical, external flow. Besides a number of empirical transition criteria and two e^N-database methods for Tollmien–Schlichting (TS) instabilities [9] and for crossflow (CF) instabilities [10], the most general transition prediction method that is currently available is a fully automated linear, local stability code named LILO [11]. The LILO code uses a frequency estimator for the detection of the relevant regions of amplified disturbances for TS instabilities and a wavelength estimator for CF instabilities. The code applies e^N methods for TS and CF waves according to the two-N-factor approach [12–15].

The RANS solver communicates the surface c_p distribution of the configuration as input data to the laminar boundary-layer method, the laminar boundary-layer method computes all of the boundary-layer parameters that are needed for the transition prediction methods, and the transition prediction methods determine new transition locations that are given back to the RANS solver. This coupled structure results in an iteration procedure for the transition locations within the iterations of the RANS equations. The structure is outlined graphically in Fig. 1.

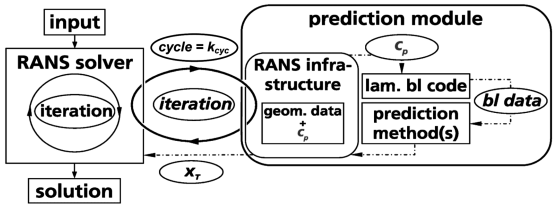

Fig. 1 Coupling structure of the RANS solver and the transition prediction module.

During the computation, the RANS solver is stopped after a certain number of iteration cycles k_{cyc}, usually when the lift has sufficiently converged, that is, when pressure oscillations have been damped to a sufficiently low degree. Then, the transition module is called, the surface data are processed, and all laminar viscous data (basically the velocity profiles in the streamwise and crossflow direction and their first and second derivatives) are calculated by the boundary-layer code. Then, either the two e^N-database methods or the stability code analyze the laminar boundary layer and try to determine a transition point. This is possible only when the transition point is located upstream of the separation point predicted by the boundary-layer code, because the boundary-layer code terminates when a separation is detected. If a transition point due to TS or CF instabilities was found, it is communicated back to the RANS solver. If no transition point due to TS or CF instabilities upstream of the laminar separation point could be found, the laminar separation point is used as approximation of the real transition point. This is an attempt to predict transition due strictly to the presence of separation bubbles. This approach often yields a good approximation of the real transition point when transition does not occur before the laminar boundary layer separates, particularly for low Reynolds number flows.

These steps are done for the upper and lower sides of all specified wing sections. When all new transition locations, $x_j^T(\mathrm{cycle} = k_{\mathrm{cyc}})$ with $j = 1, \ldots, n_T$, where n_T is the number of transition points, have been communicated back to the RANS solver, each transition location is slightly underrelaxed to damp oscillations in the convergence history of the transition locations. Then, all underrelaxed transition points (they represent a transition line on the upper or lower surface of a wing element in form of a polygonal line) are mapped onto the surface grid of the configuration applying a transition setting algorithm subdividing the surface of the geometry into laminar and turbulent regions, and the computation is continued. In so doing, the determination of the transition locations becomes an iteration process itself. With each transition location iteration step, the underrelaxation factor is reduced until a converged state of all transition points has been obtained. In the last prediction step, no underrelaxation is applied, so that the transition point value from the prediction method is considered directly and without manipulation in the following phase of the RANS computation.

The definition of a wing section is done by "line-in-flight" cuts, that is, the wing is cut through parallel to the longitudinal direction of the configuration in the global coordinate system of the RANS solver, according to strip theory.

The fixing of the predicted transition lines on the surfaces of the geometry can be performed for general three-dimensional configurations. The numerical realization of the laminar–turbulent transition is done by the limitation of the turbulence production in laminar regions and the application of point transition at the location of transition onset, that is, no transitional flow models are used.

III. Computations

A. Test Case

The three-dimensional aircraft configuration that was investigated with the TAU code, including the transition prediction module, is based on the KH3Y geometry, also called DLR F11 model. This wind-tunnel model is a half-model representing a modern transport

aircraft with a fuselage and a high-lift wing system, which can be adjusted for different flight situations. The geometric configuration used in this work was the landing configuration of the F11 model with full-span slat and flap defined in the European High-Lift Program EUROLIFT. The landing configuration exhibits a slat deflection angle of $\delta_S = 26.5\,\text{deg}$ and a flap deflection angle of $\delta_F = 32.0\,\text{deg}$. The model was experimentally tested during the EUROLIFT project in the low-speed wind tunnel of Airbus in Bremen. The aerodynamic configuration named TC214 refers to a freestream Reynolds number $Re_\infty = 1.35 \times 10^6$ (based on the reference chord length being the chord length of the wing in its retracted position at 39% of the half-span) and to freestream Mach number $M_\infty = 0.174$. In the experiments, transition detection based on hot film measurements was carried out. Two hot films were placed on the slat and the main wing elements on the outboard wing at about 68% of the half-span of the wing.

The computations were carried out for two angles of attack, $\alpha = 10.0\,\text{deg}$ and $\alpha = 14.0\,\text{deg}$, using the Spalart–Allmaras one-equation model [16] with Edwards and Chandra modification [17] (Spalart–Allmaras–Edwards = SAE) and low artificial dissipation settings $k^{(4)} = 1/64$ and $\zeta^{(\text{ratioEV})} = 0.5$, $\zeta^{(\text{ratioEV})}$ being the exponent of the eigenvalue ratios in the Martinelli coefficients. The computational grid, Fig. 2, contains about 8 million grid points and 2.24 million cells. On the solid surfaces of the geometry, about 658.000 surface cells are placed.

The stability analysis on the three elements of the wing was carried out in 9 sections on the slat, 10 sections on the upper side of the main wing element, 9 sections on the lower side of the main wing element, and 14 sections on the flap, six of which are located on the inboard part of the flap that exhibits the low sweep angle before the kink. For the lower side of the flap, fully laminar flow was assumed. The wing sections for the transition prediction on the upper sides of the wing elements are shown in Fig. 3.

The values for the critical N factors used for the stability analysis were taken from [7], in which the same configuration was investigated using a block-structured RANS code and e^N-database methods. To compare the transition prediction results from the two different code systems, the same values for the critical N factors were used. In [7], the values for the critical N factors were defined in the following way: For $\alpha = 10.0\,\text{deg}$, the hot film signals of the hot film placed on the main wing element at 68% of the half-span yielded a transition location of $(x^T/c)^{\text{main}} = 0.08$ on the upper side. In a test computation for $\alpha = 10.0\,\text{deg}$ in the corresponding wing section, only the e^N-database method for TS waves that was used in [7] yielded amplified disturbances that were high enough that transition could occur. The laminar separation point detected by the laminar boundary-layer code was located well downstream of the measured transition location $(x^T/c)^{\text{main}} = 0.08$. The e^N-database method for CF waves that was used in [7] yielded highly damped disturbances, which were not high enough for transition to occur by a CF instability. The measured transition location $(x^T/c)^{\text{main}} = 0.08$ is reached for a critical N factor for TS waves of $N^{\text{TS}}_{\text{crit}} \approx 4.9$, which corresponds to a freestream turbulence level of $Tu_\infty \approx 0.4\%$ according to Mack's relationship $N^{\text{TS}}_{\text{crit}} = -8.43 - 2.4\,\ln(Tu_\infty)$. Because there are no indications for the numerical value of the critical N factor for CF waves $N^{\text{CF}}_{\text{crit}}$ (neither from the experiments, nor from the test computation) for $N^{\text{CF}}_{\text{crit}}$ the same numerical value as for $N^{\text{TS}}_{\text{crit}}$ is applied, $N^{\text{CF}}_{\text{crit}} = N^{\text{TS}}_{\text{crit}}$. Thus, for both critical N factors $N^{\text{TS}}_{\text{crit}} = N^{\text{CF}}_{\text{crit}} = 4.9$ is used.

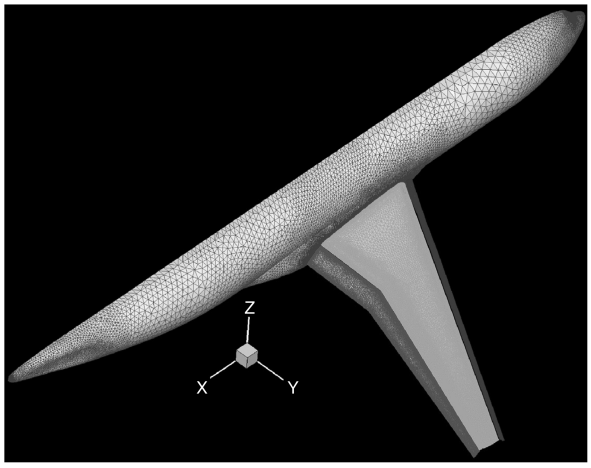

Fig. 2 Computational surface grid.

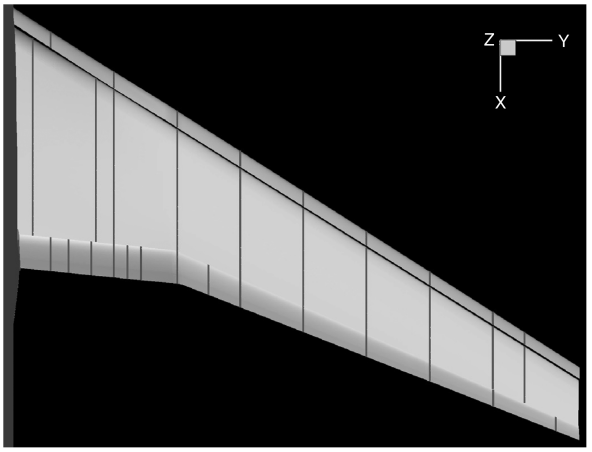

Fig. 3 Wing sections of all three wing elements (upper sides) for which transition prediction was applied.

B. Results

In Figs. 4 and 5, the predicted laminar surface regions for the upper side and lower sides, respectively, are shown for $\alpha = 10.0\,\text{deg}$ and compared with the results from [7]. In Figs. 6 and 7, the results for $\alpha = 14.0\,\text{deg}$ are compared.

Although many differences exist between the two code systems and between the different ways the setups of the two computations were arranged (hybrid code vs block-structured code, different artificial dissipation properties of the two codes, a rather fine hybrid grid vs a rather coarse block-structured grid, different positions of the wing sections, the use of grid lines of the block-structured grid as wing sections vs the use of line-in-flight cuts in the hybrid grid as wing sections, different laminar boundary-layer codes, a linear stability code vs e^N-database methods, and different techniques of fixing the predicted transition lines and mapping them onto the surface grids), for both angles of attack, the predicted transition lines are very similar for the two different approaches, the hybrid and the block-structured approach. Qualitatively, the predicted transition lines of the two different approaches are alike for both angles of attack. Quantitatively, the results show differences that are negligible, taking into account the major differences between the two approaches: the different resolutions of the wing surfaces in the chordwise as well as in the spanwise direction (depending on the corresponding wing element and the location on the wing element, the resolution in the hybrid grid is up to 10 times higher than in the block-structure grid, especially with regard to the spanwise direction) and differences in the way the transition fixing was carried out in the two approaches. There are eight regions in which the differences are particularly obvious: 1) on the slat upper side near the wing–body junction toward the fuselage, 2) on the lower sides of all elements near the wing–body junction toward the fuselage, 3) on the flap lower side in the inboard region near the fuselage, 4) on the flap lower side at the wing tip, 5) on the upper side of the main wing between the fuselage and the kink of the wing, 6) the transition line on the lower side of the main wing (the complete transition line is located visibly further downstream in the hybrid case except near the wing–body junction where it is located much further upstream and for $\alpha = 14.0\,\text{deg}$, the turbulent wedge in the hybrid case), 7) the flap upper side in the midboard region beyond the kink, where the transition line is located visibly further downstream in the hybrid case, and 8) the flap upper side directly at the wing tip in the case $\alpha = 14.0\,\text{deg}$. The reason for points 1 and 2 is the fact that, in the

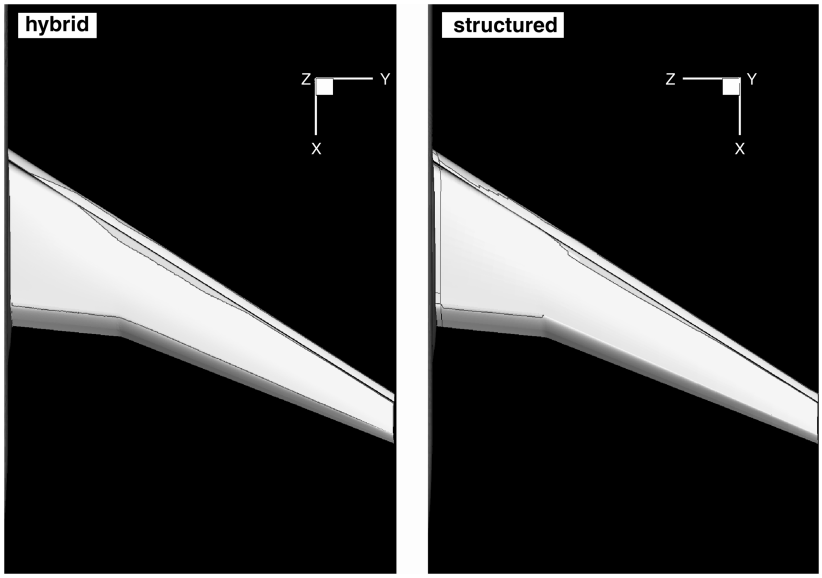

Fig. 4 Predicted laminar surface regions on the upper side of the wing for $\alpha = 10.0\,\mathrm{deg}$.

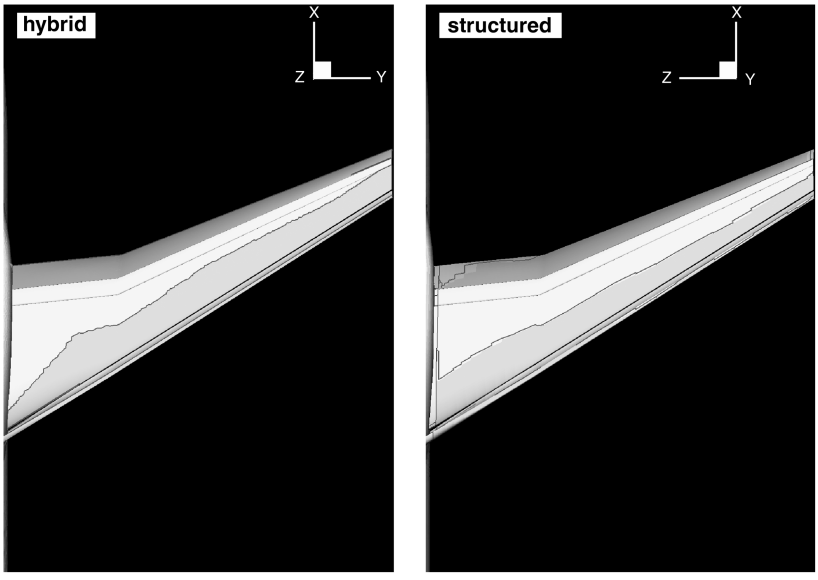

Fig. 5 Predicted laminar surface regions on the lower side of the wing for $\alpha = 10.0\,\mathrm{deg}$.

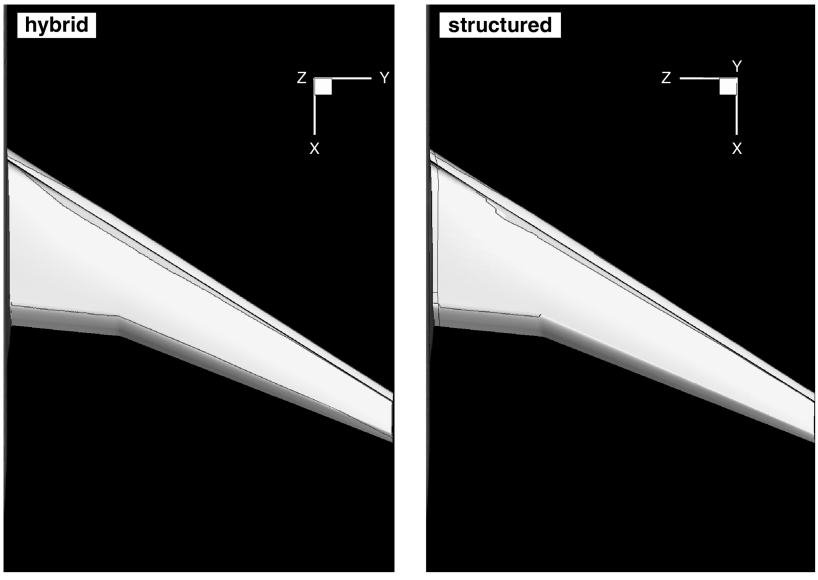

Fig. 6 Predicted laminar surface regions on the upper side of the wing for $\alpha = 14.0\,\mathrm{deg}$.

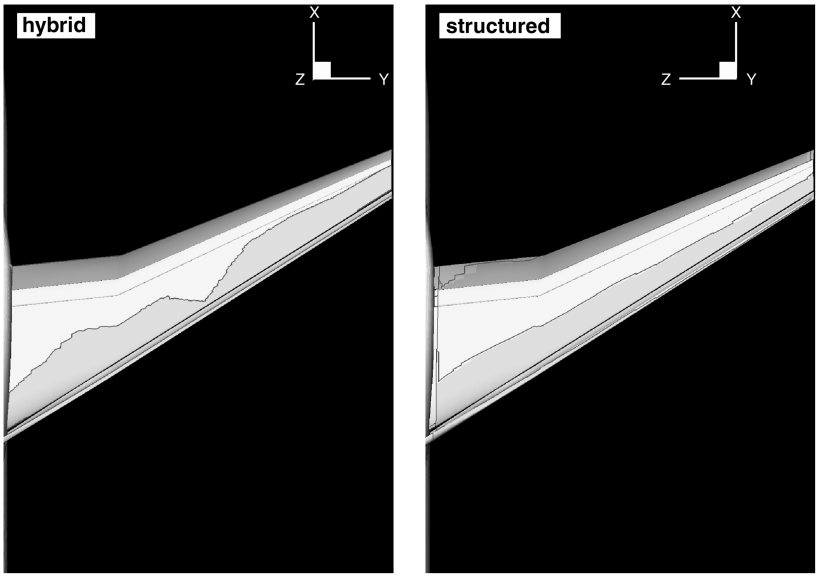

Fig. 7 Predicted laminar surface regions on the lower side of the wing for $\alpha = 14.0$ deg.

structured case in the wing grid block adjacent to the fuselage, transition was not fixed at all, but the flow was held fully turbulent in this block. The reason for points 3 and 4 is the fact that, in the hybrid case, the flap lower side was held fully laminar in contrast to the structured case. The reason for point 5 is the combination of the higher grid resolution in spanwise direction in the hybrid case and the different location of the wing sections in which the transition locations were predicted. The reasons for points 6 and 7 are unclear and are the subject of further investigations. The reason for point 8 is the fact that, in the hybrid approach, different flowfield characteristics are predicted than in the block-structured approach: For $\alpha = 14.0$ deg, an oscillation of the flowfield in the outboard region of the flap upper side leads to an oscillation of the outermost transition point of the corresponding transition line. This transition point oscillation is reflected in the laminar region at the end of the computation for $\alpha = 14.0$ deg, as depicted in Fig. 7. The oscillation of the flowfield is explained later in this paper.

In Figs. 8 and 9, the transition lines from the last four steps of the transition location iteration procedure are shown for both angles of attack. The transition iteration was started with initial transition locations that were fixed far downstream on every wing element. The laminar regions on the wing elements that are generated by these

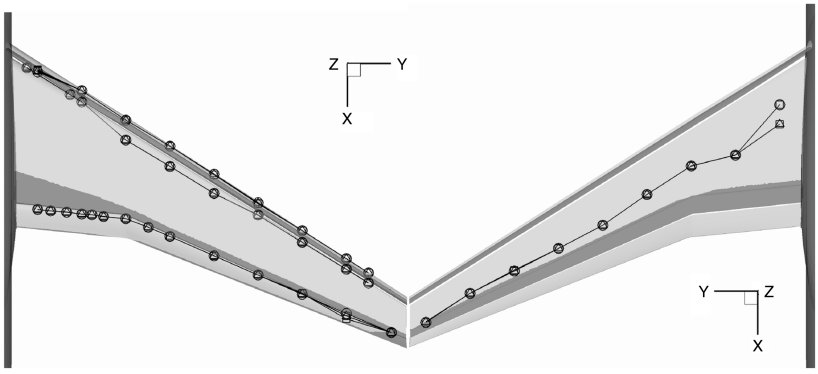

Fig. 8 Predicted transition lines from the last four steps of the transition location iteration for $\alpha = 10.0$ deg: upper side (left), lower side (right).

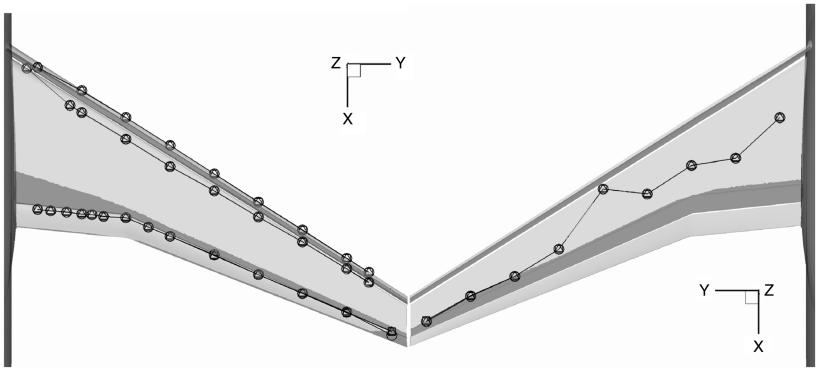

Fig. 9 Predicted transition lines from the last four steps of the transition location iteration for $\alpha = 14.0$ deg: upper side (left), lower side (right).

initial transition lines are depicted in the figures as light grey patches on the wing surface; turbulent regions are depicted as dark grey patches. After the computation was started, every 20 RANS iteration cycles, laminar separation points were searched in all the wing sections in which the transition locations are to be predicted. Because these initial transition locations do not represent the correct transition points as they would occur in reality, the RANS solution procedure reacts to this discrepancy by developing laminar separations which are detected inside the RANS grid itself by checking if reverse flow occurs in a wing section. If a laminar separation point is found, transition is fixed there and the computation is stabilized. This so-called pre-prediction phase is finished when the lift coefficient has sufficiently converged. Then, one has found a state representing a good initial guess for the transition lines on all wing elements and the real prediction phase can start. During the prediction phase, all the steps as described in Sec. II are undertaken. The RANS cycle interval for the consecutive calls of the transition prediction module was set to $\Delta k_{\text{cyc}} = 200$. The results from the last four calls are shown in the figures. The transition locations from the last call are marked by circles and those from the second-to-last call by deltas; the transition points from the other two previous calls are marked by squares. As can be seen, all transition lines are in a converged state during these last four steps of the transition iteration.

However, for $\alpha = 10.0$ deg, the innermost transition point on the slat upper side, the innermost transition point on the lower side of the main wing, and the second-to-last transition point toward the wing tip on the flap upper side and, for $\alpha = 14.0$ deg, the two outermost transition points of both the flap upper side's and the main wing lower side's transition lines are affected by oscillations that are in interaction with other oscillations within the flowfield, as can be seen in Fig. 10. There, the RANS convergence histories of the density residual, the lift coefficient, and the drag coefficient from a fully turbulent computation and from the computation with predicted transition for both angles of attack are shown. The fully turbulent computations for both angles of attack exhibit visible oscillations of all three quantities, so that it can be assumed that oscillations inside the flowfield are responsible for the oscillations of the transition points. Apparently, the local time-stepping solution scheme that is suitable for steady flows does not arrive at a steady state, but gives a hint for an unsteadiness in the problem. The convergence histories of the computations with predicted transition show that the interaction between the oscillating flowfield and the oscillating transition locations additionally perturbs the computation with a more significant impact in the case with $\alpha = 14.0$ deg.

The depictions in Figs. 11 and 12 that show the surface c_p distributions and the corresponding skin friction lines on the upper side of the wing for both angles of attack and the two different flow cases (fully turbulent vs predicted transition) indicate that the separation on the flap upper side is the main reason for this oscillation. For $\alpha = 10.0$ deg, this separation consists of a large trailing-edge separation and a short leading-edge separation bubble in the outboard part of the flap and a massive separation in the wing

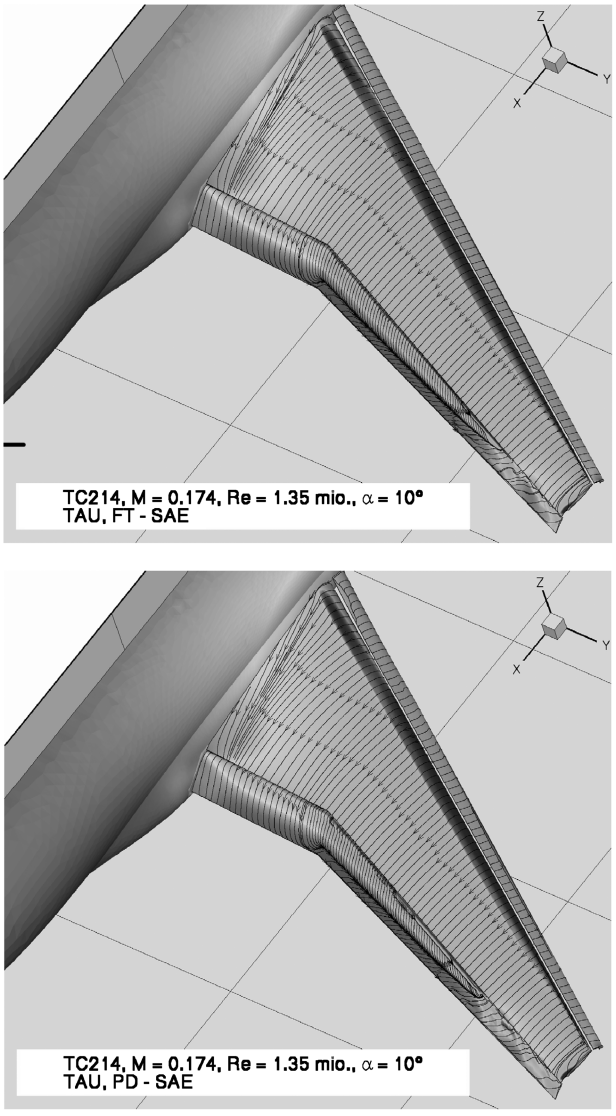

Fig. 11 Surface c_p distributions and skin friction lines for both cases on the upper side of the wing for $\alpha = 10.0$ deg, fully turbulent (top), predicted transition (bottom).

tip region of the flap. In addition, a leading-edge separation bubble in the wing tip region of the main wing element occurs. In the computation with predicted transition, all these separations are visibly larger than in the fully turbulent case. A close inspection of the case with predicted transition reveals three more separations on the upper side of the wing elements: a trailing-edge separation at the

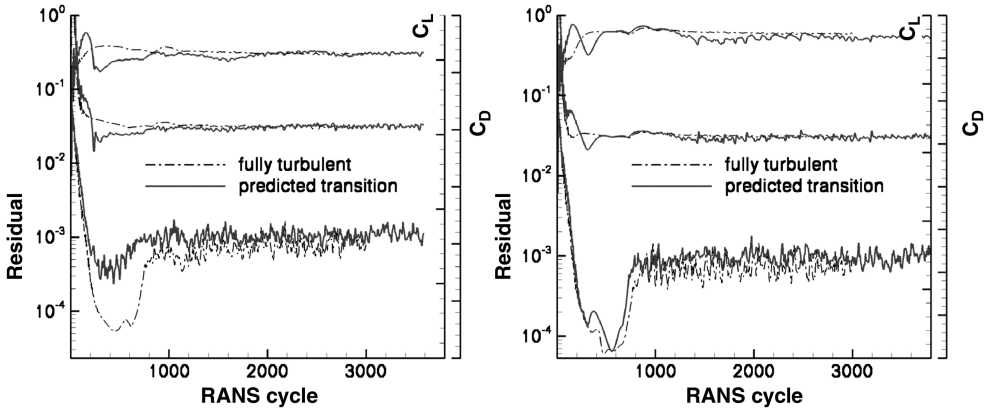

Fig. 10 RANS convergence histories for the density residual, the lift coefficient, and the drag coefficient, fully turbulent and with predicted transition: $\alpha = 10.0$ deg (left), $\alpha = 14.0$ deg (right).

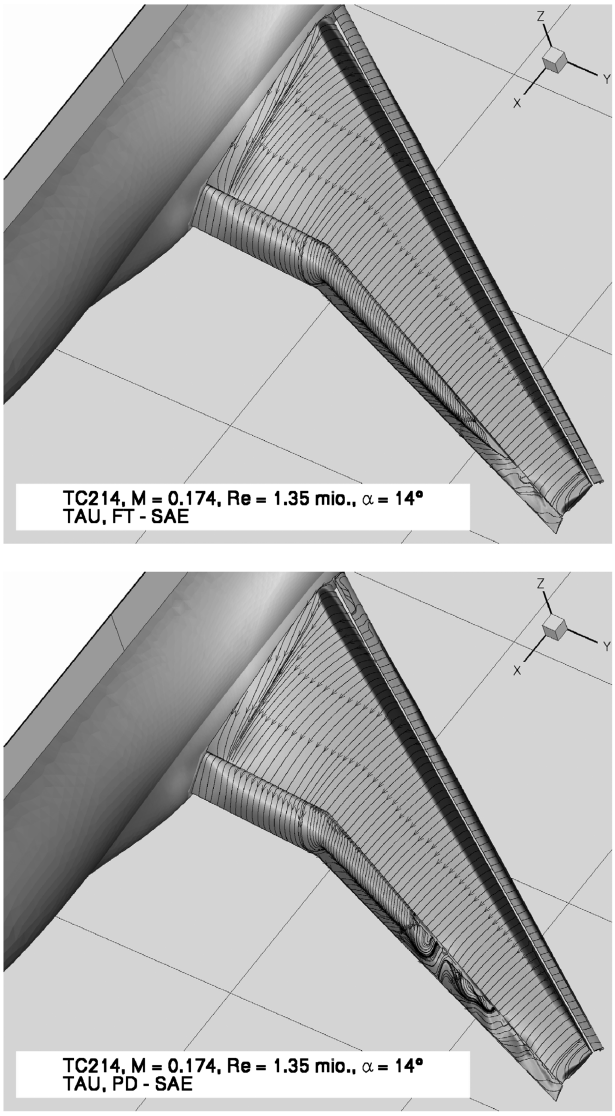

Fig. 12 Surface c_p distributions and skin friction lines for both cases on the upper side of the wing for $\alpha = 14.0$ deg, fully turbulent (top), predicted transition (bottom).

inboard slat near the fuselage, a long leading-edge separation bubble along the nose of the midboard part of the slat, and another very short leading-edge separation bubble near the kink on the flap upper side.

For $\alpha = 14.0$ deg and fully turbulent flow, the flow situation is qualitatively very similar as for $\alpha = 10.0$ deg, but another leading-edge separation bubble in the wing tip region of the main wing element has developed, which was not the case for $\alpha = 10.0$ deg. For the flow case with predicted transition, all these separations are visibly larger than in the fully turbulent case and an additional trailing-edge separation at the inboard slat near the fuselage and a long leading-edge separation bubble along the nose of the midboard part of the slat occur, as it was in the case for $\alpha = 10.0$ deg. On the flap upper side, the very complex pattern of the skin friction lines indicates that probably turbulent small-scale vortical structures emerge in that area and are washed downstream into the wake. This affect would coincide with perturbations in the convergence histories from Fig. 10, which are significantly stronger for $\alpha = 14.0$ deg. A look to the lower side of the wing in Fig. 13 for both angles of attack and the two flow cases shows the existence of another separation near the tip of the main wing.

All these separations that do not occur in the structured approach are in close interaction with the transition locations and can either affect their accuracy or can be affected by them. Thus, it is clear that there must be differences in the transition lines of the two different approaches because the basic differences in the flowfield exist in the fully turbulent solutions already.

Despite all these uncertainties, the accuracy of the predicted transition locations for those positions where experimental data are available is good. The measured transition locations on the upper sides of the slat and the main wing for the two angles of attack are given in [18] and shown in Fig. 14. There, for the two angles of attack, the predicted transition lines around that wing section where the hot films were placed during the transition measurements and the experimental transition locations are compared. The section marked with a solid line denotes the wing section where the hot films were placed. As one can see, the measured transition locations are reproduced with very good accuracy on the slat for both angles of attack and on the main wing for $\alpha = 14.0$ deg. For $\alpha = 10.0$ deg, however, one finds a visible deviation from the measured value on the main wing. Additionally, the wing section that was used for the calibration of the TS N factor in [7] is marked. This wing section (it coincides with the grid line of the bock-structured grid that is located nearest to the location of the hot films in the experiment) is marked with a dashed–double-dotted line. Comparing the predicted transition location with the transition value that was used for the calibration of the TS N factor in [7] (for this purpose, it was assumed that transition occurred in a constant relative chordwise position x^T/c in all sections), the deviation is massively smaller but still exists. At present, the reason for this deviation could not be clarified.

With regard to the conclusiveness of the predicted transition locations, the results presented are of a preliminary character, because typical transition mechanisms that can cause transition in three-dimensional flows over high-lift configurations, such as transition inside laminar separation bubbles, attachment line transition, or bypass transition when a wing component is located in the wake of an upstream located wing element, are not yet covered by the transition prediction module when the current transition prediction approach is applied. In the present case, it is very probable that attachment line transition plays a major role and can shift the

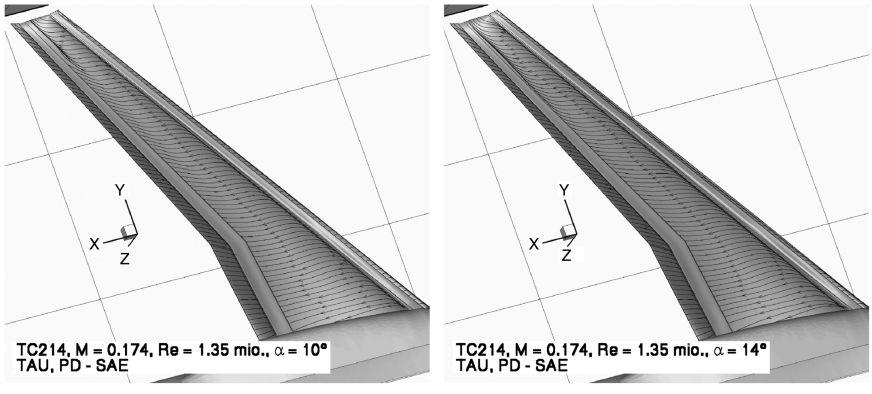

Fig. 13 Surface c_p distributions and skin friction lines for the cases with predicted transition on the lower side of the wing: $\alpha = 10.0$ deg (left), $\alpha = 14.0$ deg (right).

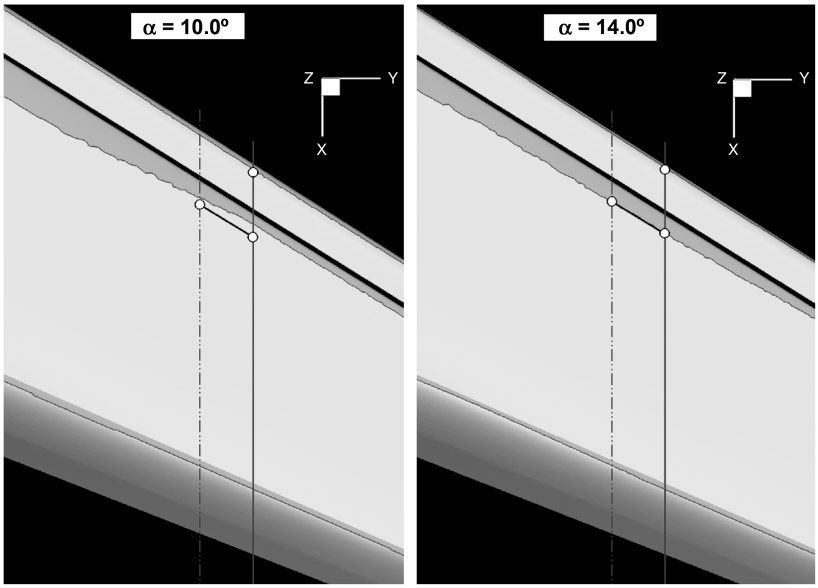

Fig. 14 Experimental transition locations and predicted transition lines in the area of the hot films.

transition lines on the slat and flap upper sides upstream so that the leading-edge separation bubbles do not occur. The incorporation of empirical or semi-empirical criteria for these transition mechanisms will be done in the near future.

Because differences exist between the hybrid and the block-structured approach, even for the fully turbulent results, influences of the different grids and of the different properties of the numerical dissipation in the two RANS codes on the solution must be investigated, especially with regard to the evolution of separations.

Finally, the comparison with experimental data has to be done to do first steps toward a physical validation of the transition prediction approach based on the coupled-code system. Before this can be done, it has to be clarified if the modeling level of the geometry is sufficiently high and if enough geometrical details are represented in the computational grid to make a proper comparison possible. It is probable that geometrical details that are missing in the present computational grid, such as slat tracks, flap tracks, and so on, have an influence on the global flowfield and on the transition locations in particular.

With respect to the applicability of the basic transition prediction strategy of the coupled-code system, it could be shown that the automated coupling of a RANS solver, a laminar boundary-layer code, and an accurate stability analysis tool yields transition locations of comparable high accuracy regardless of which specific codes are used.

IV. Conclusions

A hybrid Reynolds-averaged Navier–Stokes solver with automatic transition prediction functionality was successfully applied to an industrially relevant wing–body high-lift aircraft configuration with a three-element wing consisting of a main wing with full-span slat and flap. The RANS solver which is coupled to a transition prediction module represents a simulation system that predicts the unknown transition locations during the ongoing RANS computation iteratively in an automatic manner without intervention of the code user. The transition prediction module contains a laminar boundary-layer code for swept, tapered wings and compressible, conical external flow and a fully automated local, linear stability code for the prediction of transition due to Tollmien–Schlichting and crossflow instabilities using the e^N method based on the two-N-factor approach.

The computations were carried out for two angles of attack, $\alpha = 10.0\,\text{deg}$ and $\alpha = 14.0\,\text{deg}$, for fully turbulent flow and flow with predicted transition lines. The results were compared with results obtained with another coupled system based on a block-structured Reynolds-averaged Navier–Stokes solver. It could be shown that the predicted transition lines are qualitatively alike. Quantitatively, the results show differences that are negligible, taking into account the differences between the codes system based on the hybrid solver and the one based on the block-structured solver.

Although typical transition mechanisms that can occur in three-dimensional high-lift flows are not yet covered, such as attachment line transition, the main objective, which was to demonstrate that the underlying transition prediction procedure embedded in the DLR, German Aerospace Center TAU code is capable of being applied to complex high-lift aircraft configurations of industrial relevance, was achieved.

Acknowledgments

The authors thank the consortium of the European High-Lift Program II project [19] for letting them use the geometry of the TC214 configuration. This project was a collaboration between DLR, German Aerospace Center, Airbus, Alenia Aeronautica S.p.A., Dassault Aviation, Centro Italiano Ricerche Aerospaziali S.C.p.A., European Transonic Wind Tunnel GmbH, Ingenieurbüro Dr. Kretschmar, Instituto Nacional de Tecnica Aeroespacial, ONERA, Stichting Nationaal Lucht- en Ruimtevaart Laboratorium, and the Swedish Defense Research Agency. The project was managed by the DLR, German Aerospace Center and was partly funded by the European Union (project reference GRD-2004-502896).

References

[1] TAU-Code User Guide, Release 2007.1.0, Inst. of Aerodynamics and Flow Technology, DLR, German Aerospace Center, Göttingen, Germany, April 2007.

[2] Schwamborn, D., Gerhold, T., and Hannemann, V., "On the Validation of the DLR-TAU Code," *New Results in Numerical and Experimental Fluid Mechanics II*, Notes on Numerical Fluid Mechanics, Vol. 72, Vieweg, Brunswick, Germany, 1999, pp. 426–433.

[3] Kroll, N., Rossow, C.-C., Schwamborn, D., Becker, K., and Heller, G., "MEGAFLOW: A Numerical Flow Simulation Tool for Transport Aircraft Design," *International Council of the Aeronautical Sciences Congress 2002* [CD-ROM], International Council of the Aeronautical Sciences, Toronto, Canada, 2002, pp. 1.105.1–1.105.20.

[4] Schwamborn, D., Gerhold, T., and Heinrich, R., "The DLR TAU-Code: Recent Applications in Research and Industry," *European Conference on Computational Fluid Dynamics, ECCOMAS CFD 2006* [CD-ROM], edited by P. Wesseling, E. Oñate, J. Périaux, Technical Univ. of Delft, The Netherlands, 2006, ISBN 90-9020970-0.

[5] Krumbein, A., "Automatic Transition Prediction and Application to High-Lift Multi-Element Configurations," *Journal of Aircraft*, Vol. 42, No. 5, 2005, pp. 1150–1164.

doi:10.2514/1.10329; also AIAA Paper 2004-2543, June/July 2004.

[6] Krumbein, A., "Automatic Transition Prediction and Application to Three-Dimensional Wing Configurations," *Journal of Aircraft*, Vol. 44, No. 1, 2007, pp. 119–133.
doi:10.2514/1.22254; also AIAA Paper 2006-914, Jan. 2006.

[7] Krumbein, A., "Automatic Transition Prediction and Application to Three-Dimensional High-Lift Configurations," *Journal of Aircraft*, Vol. 44, No. 3, 2007, pp. 918–926.
doi:10.2514/1.25528 ;also AIAA Paper 2006-3164, June 2006.

[8] "COCO: A Program to Compute Velocity and Temperature Profiles for Local and Nonlocal Stability Analysis of Compressible, Conical Boundary Layers with Suction," Center of Applied Space Technology and Microgravity Technical Rept., Nov. 1998.

[9] Stock, H. W., and Degenhardt, E., "A Simplified e^N Method for Transition Prediction in Two-Dimensional, Incompressible Boundary Layers," *Zeitung für Flugwissenschaft und Weltraumforschung*, Vol. 13, 1989, pp. 16–30.

[10] Casalis, G., and Arnal, D., "ELFIN II Subtask 2.3, Database Method: Development and Validation of the Simplified Method for Pure Crossflow Instability at Low Speed," ELFIN II—European Laminar Flow Investigation, TR 145, ONERA R.T. DERAT No. 119/5618.16, Dec. 1996.

[11] Schrauf, G., "LILO 2.1 User's Guide and Tutorial," Geza Schrauf Stability Computations Technical Rept. 6, originally issued Sept. 2004, modified for Ver. 2.1 July 2006.

[12] Rozendaal, R. A., "Natural Laminar Flow Flight Experiments on a Swept Wing Business Jet-Boundary-Layer Stability Analysis," NASA CP 3975, March 1986.

[13] Rozendaal, R. A., "Variable-Sweep Transition Flight Experiment (VSTFE): Parametric Pressure Distribution Boundary-Layer Stability Study and Wing Glove Design Task," NASA CR 3992, Dec. 1986.

[14] Rozendaal, R. A., "Variable-Sweep Transition Flight Experiment (VSTFE): Stability Code Development and Clean-Up Glove Analysis," NASA CP 2847, April 1987.

[15] Schrauf, G., "Large-Scale Laminar-Flow Tests Evaluated with Linear Stability Theory," *Journal of Aircraft*, Vol. 41, No. 2, March–April 2004, pp. 224–230.
doi:10.2514/1.9280

[16] Spalart, P. R., and Allmaras, S. R., "A One-Equation Turbulence Model for Aerodynamic Flows," *Recherche Aérospatiale*, Vol. 1, 1994, pp. 5–21.

[17] Edwards, J. R., and Chandra, S., "Comparison of Eddy Viscosity-Transport Turbulence Models for Three-Dimensional, Shock-Separated Flowfields," *AIAA Journal*, Vol. 34, No. 4, 1996, pp. 756–763.
doi:10.2514/3.13137

[18] Schrauf, G., "EUROLIFT II Task 1.2: On the Evaluation of the EUROLIFT Low-Speed Wind-Tunnel Tests," Deutsche Aerospace Airbus Presentation Charts, Dec. 2004.

[19] "EUROLIFT II: European High-Lift Program II, Annex B: Description of Work," *A Specific Targeted Research Project of the 6th European Framework Program*, GRD-2004-502896, 2004.